

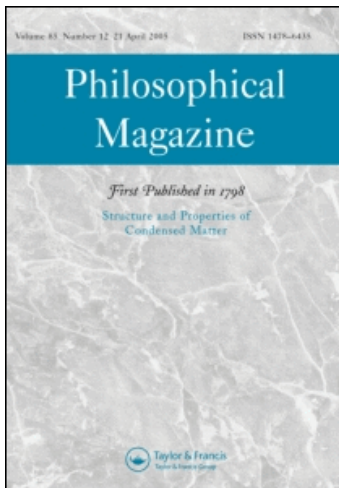
This article was downloaded by: [CAS Chinese Academy of Sciences]

On: 14 August 2010

Access details: Access Details: [subscription number 906076485]

Publisher Taylor & Francis

Informa Ltd Registered in England and Wales Registered Number: 1072954 Registered office: Mortimer House, 37-41 Mortimer Street, London W1T 3JH, UK



Philosophical Magazine

Publication details, including instructions for authors and subscription information:

<http://www.informaworld.com/smpp/title~content=t713695589>

Cyclic deformation and fatigue damage behaviors of oriented Ag single crystal

P. Li^a; Z. F. Zhang^a; S. X. Li^a; Z. G. Wang^a

^a Shenyang National Laboratory for Materials Science, Institute of Metal Research, Chinese Academy of Sciences, 110016, Shenyang, P.R. China

To cite this Article Li, P. , Zhang, Z. F. , Li, S. X. and Wang, Z. G.(2009) 'Cyclic deformation and fatigue damage behaviors of oriented Ag single crystal', Philosophical Magazine, 89: 32, 2903 – 2920

To link to this Article: DOI: 10.1080/14786430903130847

URL: <http://dx.doi.org/10.1080/14786430903130847>

PLEASE SCROLL DOWN FOR ARTICLE

Full terms and conditions of use: <http://www.informaworld.com/terms-and-conditions-of-access.pdf>

This article may be used for research, teaching and private study purposes. Any substantial or systematic reproduction, re-distribution, re-selling, loan or sub-licensing, systematic supply or distribution in any form to anyone is expressly forbidden.

The publisher does not give any warranty express or implied or make any representation that the contents will be complete or accurate or up to date. The accuracy of any instructions, formulae and drug doses should be independently verified with primary sources. The publisher shall not be liable for any loss, actions, claims, proceedings, demand or costs or damages whatsoever or howsoever caused arising directly or indirectly in connection with or arising out of the use of this material.

Cyclic deformation and fatigue damage behaviors of $[\bar{1}414]$ oriented Ag single crystal

P. Li, Z.F. Zhang*, S.X. Li and Z.G. Wang

Shenyang National Laboratory for Materials Science, Institute of Metal Research, Chinese Academy of Sciences, 72 Wenhua Road, 110016, Shenyang, P.R. China

(Received 16 January 2009; final version received 19 June 2009)

The cyclic deformation and fatigue damage behaviors of $[\bar{1}414]$ oriented Ag single crystal were investigated in terms of cyclic stress–strain (CSS) curves, surface slip morphologies and dislocation configurations. A clear plateau region appears in the CSS curve of the $[\bar{1}414]$ Ag single crystal over a strain range of $\gamma_{pl} = 1.5 \times 10^{-4} - 4 \times 10^{-3}$ with average saturation shear stress amplitude of ~ 26.6 MPa. Corresponding ladder-like persistent slip bands (PSBs) also appear in the $[\bar{1}414]$ Ag single crystal. Compared with other Cu and Ag single crystals with single or double-slip orientations, the saturation resolved shear stresses of the critical double-slip-oriented single crystals, no matter whether for Cu or Ag, are significantly higher than that of the single-slip-oriented ones. Combining the two-phase model with the hindering effect of sessile jogs on screw dislocation movement, a three-phase model is proposed to rationalize the increase of saturation stress. In addition, the surface slip morphologies of the $[\bar{1}414]$ Ag single crystal were characterized by the interactions between the primary and secondary SBs. According to the difference in their slippage, their interactions can be divided into three types, which could simultaneously appear in different local areas of the same crystal. The current experimental results extend the fundamental understanding of the intrinsic fatigue damage behaviors of fcc metal crystals.

Keywords: silver single crystal; cyclic stress–strain curve; persistent slip band; sessile jog; two-phase model

1. Introduction

Systematic research on the cyclic deformation behavior of fcc metal crystals started with Cu single crystals. During the second half of the last century, especially during the 1960s–1980s, researchers paid much attention to the cyclic deformation and fatigue damage behaviors of single-slip-oriented Cu single crystals. In this period, one of the most distinguishing findings is perhaps the cyclic stress–strain (CSS) saturation behavior. This saturation behavior, in fact, has two meanings: the first is

*Corresponding author. Email: zhfzhang@imr.ac.cn.

the cyclic saturation observed in the cyclic hardening curve [1] and the second refers to the plateau behavior in the CSS curve. The other interesting finding is that persistent slip bands (PSBs) with a ladder-like structure always nucleated after cyclic saturation of copper single crystals. Meanwhile, a two-phase (PSBs and matrix) model was proposed to explain the distribution of plastic strain localization within PSBs and matrix in fatigued Cu single crystal [2,3]. In 1978, Mughrabi [4] first determined the plateau behavior from experiment and divided the CSS curve into three regions according to the evolution of dislocation configurations. In the plateau region, the plastic strain is mainly localized in the narrow PSBs with a saturation resolved shear stress of about 28 MPa. From then on, it was generally accepted that both the saturation and plateau behaviors are related to the formation and development of PSBs.

During 1980s–1990s, based on the deep understanding of single-slip-oriented Cu single crystals, Jin [5] and Jin and Winter [6] studied preliminarily the CSS responses and dislocation structures of Cu single crystals with $[012]$, $[\bar{1}12]$ and $[\bar{1}22]$ double-slip orientations on the three sides of the stereographic triangle at a relatively high strain amplitude of 3.0×10^{-3} . Based on the CSS responses and dislocation structures, Jin [7,8] proposed a set of dislocation interaction models and divided the crystallographic triangle into several different regions according to the model. In different regions, the slip deformation and dislocation interactions have different types [8], which successfully explained the different cyclic deformation behaviors of double-slip-oriented and multi-slip-oriented crystals (see Figure 1b).

Thereafter, the results of Gong et al. [9,10] further confirmed that these differences are related to the modes and the intensities of dislocation interactions, i.e. the formation of Lomer–Cottrell locks in $[\bar{1}12]$ crystals, sessile jogs in $[012]$ crystals and new glissile coplanar dislocations in $[\bar{1}22]$ crystals. More recently, Li et al. [11,12] focused on the dislocation structures of cyclically deformed conjugate, critical and coplanar double-slip-oriented Cu single crystals in a wide

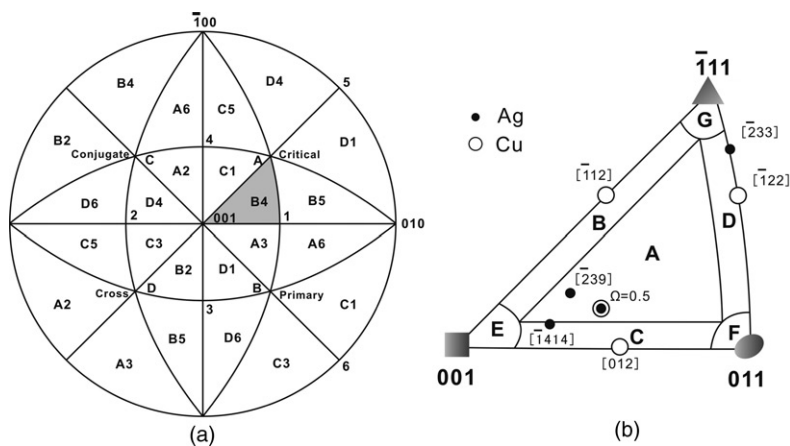


Figure 1. Orientation of crystals investigated and various dislocation structures formed in differently oriented crystals: (a) notation of crystal planes and axes; (b) stereographic triangle.

range of strain amplitudes. It was found that the crystallographic orientation had a notable effect on the dislocation structures in cyclically saturated critical or coplanar double-slip-oriented Cu single crystals, but nearly no effect on the dislocation structure in the conjugate double-slip-oriented Cu single crystals. Usually, Lomer–Cottrell locks can effectively prevent the interactions of the subsequent dislocations, but for sessile jogs and new glissile dislocations, it is difficult to avoid further interactions with the primary dislocations, which is the main reason that different double-slip-oriented Cu single crystals show various dislocation configurations.

Apart from Cu single crystals, Ni single crystals can be regarded as the second fcc metal crystals investigated widely. The results from Bretschneider et al. [13] showed that the cyclic deformation behaviors of Ni single crystals oriented for single slip were consistent with those of Cu single crystals, apart from higher saturation resolved shear stress (50 MPa). Subsequently, Buque [14] further systematically studied the effect of the grain orientation on the saturated dislocation structures of fine-grained Ni polycrystals. They found that the main features of the dislocation configuration in an individual grain were essentially determined by the crystallographic axial orientation of the grain. The labyrinth type, the patch type and the fragmented wall type were found for grains with the orientations of [001], [011] and $[\bar{1}11]$, respectively. The results are still similar to those of Cu crystals.

In summary, although many review papers [15–19] have been published and summarized, the results of an extensive work done over the past half of the century, the cyclic deformation and fatigue damage behaviors of fcc metal crystals at low amplitudes are still attracting much attention, which can be attributed to at least the following three reasons:

- (1) The comprehension of cyclic deformation behaviors in fcc single crystals with single slip orientations provides fundamental ideas for the understanding of the fatigue behavior of double- and even multiple-slip-oriented single crystals.
- (2) In spite of the large amount of experimental data and of many promising modeling approaches available, basic physical mechanisms determining the cyclic deformation behavior are still not known in sufficient detail.
- (3) Not only are there many fcc metal crystals, such as Au and Ag, for which the cyclic deformation behaviors remain unknown, but also the cyclic deformation behaviors, especially dislocation configurations of various fcc metal crystals that have been investigated widely, are not the same.

Based on the above facts, this paper reports the use of a $[\bar{1}414]$ Ag single crystal as a model material to establish its CSS curve and compare it with that of Cu single crystal with single-slip orientation [4]. The second purpose of the present paper is to find out whether the regular dislocation configurations, especially ladder-like PSBs, can appear in Ag single crystal or not. Since the cyclic deformation behaviors of $[\bar{1}414]$ Ag single crystal with orientation close to critical double slip are mainly affected by dislocation interactions, it is necessary to re-describe the fatigue model from a new perspective for better understanding of the complex interactions of dislocations in terms of the traditional two-phase model. Hence, this paper will provide a more systematic investigation on the fatigued Ag single crystal on the basis

of former papers [20,21], with the aim of continuously expanding the extent of macroscopic deformation behaviors (including CSS curves and surface slip morphologies) and microscopic dislocation configurations in fcc metals.

2. Experimental procedures

A bulk single crystal was grown from electrolytic Ag of 99.999% purity by the Bridgman method. Some fatigue specimens with dimensions of 7 mm × 5 mm × 54 mm and a gauge section of 5 mm × 5 mm × 16 mm were cut by an electron-spark cutting machine. The crystal orientation (**G**) of the specimen was determined by the electron back-scattering diffraction (EBSD) technique with the accuracy within ±2° in a Cambridge S360 scanning electron microscope (SEM), with the following results:

$$\mathbf{G} = \begin{bmatrix} \overline{0.9089} & \overline{0.2806} & \overline{0.3084} \\ 0.2410 & \overline{0.9571} & \overline{0.1606} \\ \overline{0.3403} & 0.0716 & \overline{0.9376} \end{bmatrix} \approx \begin{bmatrix} \overline{13} & \overline{4} & \overline{4} \\ 3 & \overline{14} & \overline{2} \\ \overline{5} & 1 & \overline{13} \end{bmatrix},$$

where (−0.2806, −0.9571, 0.0716) corresponds to the crystal orientation parallel to the loading axis; in brief, it can be referred to as an orientation $[\overline{1}414]$ in a standard stereographic triangle for comparison with previous work [20–22]. In the crystal, four slip systems are shown in Figure 1a and the corresponding dislocation reaction model and formed dislocation patterns are listed in Table 1. Based on the classification of slip systems, the $[\overline{1}414]$ orientation locates at the junction of the single-slip region and the critical double-slip one with a Schmid factor of about 0.488. Hereafter, the Ag and Cu single crystals with different slip systems involved in this work are as summarized in Figure 1b.

Before fatigue testing, all the specimens were electrolytically polished to produce a strain-free surface for microscopic observations. In the process of loading, the errors in aligning the specimens within the loading axis are minimized to ±1°. Then the specimens were deformed cyclically in fully reversed push–pull on a Shimadzu servohydraulic testing machine under constant plastic strain control at room temperature in air. The plastic strain resolution and control precision are less than 10^{−5}. A triangle wave with a frequency of 0.5 Hz was used. All specimens were deformed cyclically up to the occurrence of saturation. After the fatigue tests, the surface slip morphologies and dislocation configurations were carefully observed by the scanning electron microscopy (SEM) and the electron channeling contrast (ECC) technique, respectively. Such ECC images are similar in appearance to transmission electron micrographs, albeit with a lower image resolution [23–26]. However, the ECC technique in SEM has a great advantage in the observations of fatigued dislocation patterns in a larger area, especially near grain boundaries, deformation bands or fatigue cracks [27–30]. More detailed dislocation configurations, especially PSB walls, were investigated with the Tecnai G2 F30 transmission electron microscope (TEM).

Table 1. Dislocation interaction characteristic and formed dislocation structures corresponding to different regions.

Region		Most highly stressed slip system	Characteristic of dislocation reaction	Dislocation structure
Single slip	A	$B4(111)\bar{1}01$	—	PSB ladders and matrix vein
Conjugate double slip	B	$B4(111)\bar{1}01$ $C1(\bar{1}\bar{1}1)[011]$	Lomer–Cottrell lock	PSB ladders and matrix vein formed in each separated region
Critical double slip	C	$B4(111)\bar{1}01$ $A3(111)[101]$	Sessile jog	Interacted PSB ladders or labyrinth-like structure
Coplanar double slip	D	$B4(111)\bar{1}01$ $B5(111)\bar{1}10$	New glissile in (111)	Cell-like structure
	E	$\bar{1}01$ and $[101]$ $0\bar{1}1$ and $[011]$	Non-coplanar dislocation intersections	Labyrinth-like structure
Multiple slip	F	$B4(111)\bar{1}01$ $A3(111)[101]$ $B5(111)\bar{1}10$ $A6(111)[110]$	Non-coplanar dislocation intersections and coplanar dislocation reaction	Dislocation cells, $\{100\}$ dislocation walls, labyrinth and PSB ladders
	G	$B5(111)\bar{1}10$ $D1(\bar{1}\bar{1}1)[011]$ $C5(\bar{1}\bar{1}1)[110]$	Activation of secondary slip systems	Cells and labyrinth-like structures

3. Experimental results

3.1. Cyclic hardening and saturation behaviors

Figure 2 shows cyclic hardening curves of the $[\bar{1}414]$ Ag single crystal deformed at different strain amplitudes. Fatigue testing conditions and data of cyclic hardening and saturation stresses are listed in Table 2, where γ_{pl} is the constant plastic shear strain amplitude, $\gamma_{pl,cum}$ ($\gamma_{pl,cum} = 4N\gamma_{pl}$, N is the number of cycles) is the cumulative plastic shear strain, τ_s is the saturation resolved shear stress, τ_{max} is the maximum resolved shear stress and $R = \tau_{max}/\tau_s$ is a parameter describing cyclic softening behavior. Taken the cumulative plastic shear strain as a reference, combined with some empirical rules. (For example the cycles required for high strain amplitude are usually higher than expected. However, at low strain amplitude, the cycles are lower than that expected), the cycles to reach the saturation at different strain amplitude can be well estimated.

As can be seen from Figure 2, the cyclic stress response curves of the $[\bar{1}414]$ Ag single crystal at various plastic strain amplitudes can be divided into three groups according to the stress overshooting behavior. (i) When $\gamma_{pl} \leq 5 \times 10^{-4}$, the curves exhibit a slight stress overshooting stage and the amount of overshooting decreases with increasing γ_{pl} . (ii) When $\gamma_{pl} = 1 \times 10^{-3} - 2 \times 10^{-3}$, after the initial cyclic hardening, the shear stress directly enters into a saturation state, showing a negligible

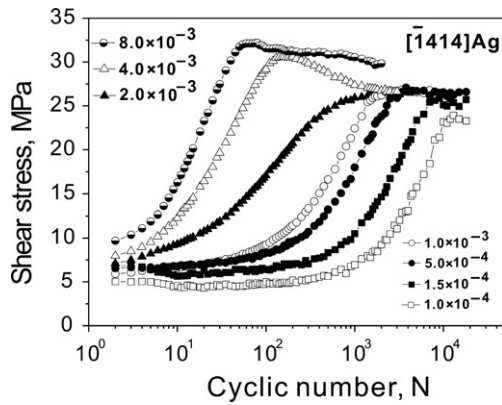


Figure 2. Cyclic hardening curves of the $[\bar{1}414]$ Ag single crystal at different plastic resolved shear strain amplitudes.

Table 2. Fatigue testing conditions and data for $[\bar{1}414]$ Ag single crystal.

Specimen No.	γ_{pl}	Cyclic No.	$\gamma_{pl,cum}$	τ_s (MPa)	τ_{max} (MPa)	$R = \tau_{max}/\tau_s$
1	1×10^{-4}	50,000	10	23.2	23.9	1.03
2	1.5×10^{-4}	40,000	12	25.2	25.8	1.02
3	5×10^{-4}	20,000	20	26.6	27.1	1.02
4	1×10^{-3}	10,000	20	26.6	26.8	1.00
5	2×10^{-3}	4000	16	26.5	26.7	1.00
6	4×10^{-3}	3000	24	26.65	30.6	1.15
7	8×10^{-3}	2000	32	28.6	32.1	1.12

stress overshooting. (iii) At higher strain amplitudes ($\gamma_{pl} \geq 4 \times 10^{-3}$), an obvious stress overshooting stage occurs again, and the amount of overshooting still decreases with γ_{pl} increasing. In Table 2, $R = \tau_{max}/\tau_s$ reflects the degree of the stress overshooting of the Ag single crystals cyclically deformed at different strain amplitudes. The above stress overshooting behavior is similar to that of the $[011]$ or $[\bar{1}12]$ Cu single crystal [31,32], but different from that of the $[017]$ or $[\bar{2}33]$ Cu single crystal [33,34].

3.2. Cyclic stress–strain (CSS) curves

The CSS curves of the $[\bar{1}414]$ Ag single crystal and the single-slip-oriented Cu single crystal from Mughrabi [4] are shown in Figure 3. By comparison, it is interesting to find that the CSS curve of the $[\bar{1}414]$ Ag single crystal also shows a clear plateau region over a strain range of $\gamma_{pl} = 1.5 \times 10^{-4} - 4 \times 10^{-3}$ with an average saturation stress of ~ 26.6 MPa, which is slightly lower than that (~ 28 MPa) of single-slip-oriented Cu single crystal with the Schmid factor of 0.5 from Mughrabi [4]. The plateau region for the $[\bar{1}414]$ Ag single crystal is also slightly shorter than that of Cu

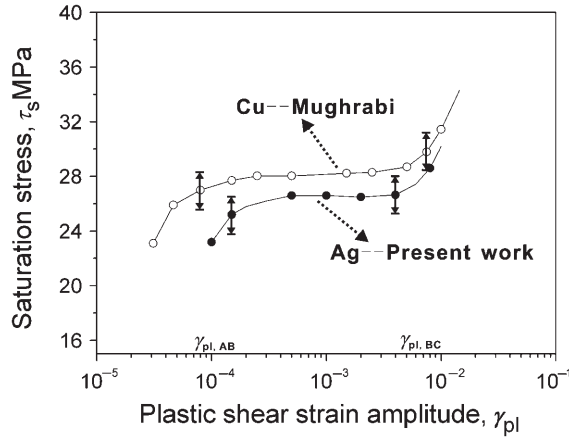


Figure 3. Cyclic stress–strain curves of Ag and Cu single crystals. (Note: $\gamma_{pl,AB}$ and $\gamma_{pl,BC}$ are the strain amplitudes corresponding to the start point and end point of the plateau region in the CSS curves, respectively).

Table 3. Cyclic stress–strain data of Cu and Ag single crystals with different single- and double-slip orientations.

Metal (orientation)	$\gamma_{pl,AB}$	$\gamma_{pl,BC}$	τ_s (MPa)	Investigators
Cu (single slip)	6.0×10^{-5}	7.5×10^{-3}	27.5	Mughrabi [4]
Cu ($[\bar{1}12]$ con)	5.0×10^{-4}	4.0×10^{-3}	28.6	Li et al. [32]
Cu ($[012]$ cri)	$\gamma_{pl} = 3.0 \times 10^{-3}$		31.4	Jin [5]
Cu ($[122]$ cop)	$\gamma_{pl} = 3.0 \times 10^{-3}$		35.8	Jin [6]
Ag (single slip)	6.0×10^{-5}	7.5×10^{-3}	17.5	Mughrabi et al. [22]
Ag ($\sim[113]$ con)	$\gamma_{pl} = 2.1 \times 10^{-3}$		18	Li et al. [21]
Ag ($\sim[027]$ cri)	1.5×10^{-4}	4.0×10^{-3}	26.6	Present result
Ag ($[233]$ cop)	1.35×10^{-4}	2.7×10^{-3}	25	Li et al. [20]

single crystal and similar to that for the $[\bar{2}33]$ Ag single crystal [20]. In addition, the CSS data of the above single crystals were summed up with those of other Cu and Ag single crystals with single- or double-slip orientations together, as listed in Table 3. It can be seen that the saturation resolved shear stresses of the conjugate double-slip-oriented single crystals, no matter whether for Cu or Ag, are equivalent to that of single-slip-oriented single crystals [4,21,22,32]. However, the saturation resolved shear stress of the critical or coplanar double-slip-oriented single crystals is significantly higher than that of the single-slip-oriented ones, which will be discussed later.

3.3. Surface slip features and dislocation configurations

Figure 4 shows the surface slip morphologies of the $[\bar{1}414]$ Ag single crystal cyclically deformed to saturation at different strain amplitudes. After the sample

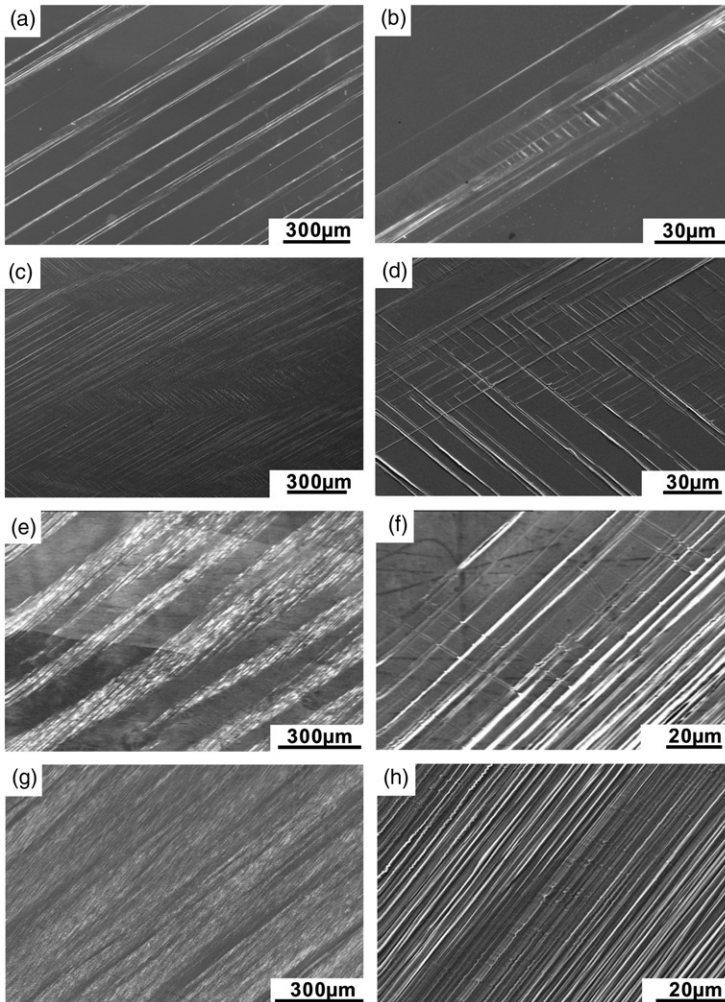


Figure 4. Surface slip morphologies of the $[1\ 4\ 14]$ Ag single crystal cyclically deformed at various strain amplitudes: (a, b) $\gamma_{pl} = 1.0 \times 10^{-4}$; (c, d) $\gamma_{pl} = 5.0 \times 10^{-4}$; (e, f) $\gamma_{pl} = 2.0 \times 10^{-3}$; (g, h) $\gamma_{pl} = 8.0 \times 10^{-3}$.

reaches saturation, the surface morphologies are not greatly affected by the next number of cycles or the cumulative plastic shear strain. Therefore, the decisive factor to influence the surface morphologies of Ag single crystal is only the strain amplitude. At the lower strain amplitude of 1.0×10^{-4} (see Figure 4a), the specimen surface is mainly comprised of the primary slip bands (SB), supplemented by the weak secondary SBs in local regions (see Figure 4b). With increasing strain amplitude to 5.0×10^{-4} , both the primary and secondary SBs become dense and the interactions between them become notable, as shown in Figures 4c and 4d. When $\gamma_{pl} = 2.0 \times 10^{-3}$, the primary SBs become denser and denser, but the secondary SBs are relatively loose (see Figures 4e and 4f), indicating that the development of the

secondary SBs is constrained by that of the primary SBs and further evolution stops above this strain amplitude. By further increasing strain amplitude to 8.0×10^{-3} , the primary SBs are highly concentrated and almost covered with the whole specimen surface, as shown in Figures 4g and 4h. Meanwhile, the secondary SBs become weaker and weaker, even almost disappearing. The fundamental reason for this phenomenon can be attributed to the inhibition effect of the primary SBs on the secondary SBs. During the cyclic deformation, the primary slip system was firstly operated and the secondary slip system became active later. At lower strain amplitude, the inhibition effect should be very weak. With increasing strain amplitude, the inhibition becomes gradually obvious, accompanying continuous expansion of the secondary SBs. Above a critical strain amplitude, the inhibition of the primary SBs on the secondary SBs exceeds the expansion of the secondary SBs, as a result, it seems that the secondary SBs is weakened.

It has already been shown that when $\gamma_{pl} = 5.0 \times 10^{-4}$, the interactions between the primary and secondary SBs are most apparent. Accordingly, in order to better analyze the interactions of SBs, the dislocation configurations of specimen cyclically deformed at this strain amplitude were carefully observed by SEM–ECC and are shown in Figure 5. It can be seen that the sample surface was completely covered with the PSBs. At different magnifications, Figures 5c–5h enable more close comparisons. It is apparent that the distribution of PSBs is in good agreement with the primary and secondary SBs, which further confirms that the PSB-ladder structures indeed exist in the Ag single crystal, as widely observed in Cu single crystals. More detailed information can be obtained elsewhere [21] and in Section 4.3.

4. Discussion

4.1. Saturation resolved shear stresses and surface slip morphology

According to the analysis from Section 3.2 and Table 3, it has been shown that, on the one hand, the CSS curve of the $[\bar{1}414]$ Ag single crystal shows a clear plateau region, whereas on the other hand the corresponding saturation shear stress is 7–8 MPa higher than that of Ag single crystal with single-slip orientation. Therefore, it can be more accurately stated that the $[\bar{1}414]$ Ag single crystal possesses both some characteristics of single-slip-oriented crystals and some features of critical double-slip-oriented crystals. Based on this understanding, the reason for the increase of the saturation shear stress will be given. As shown in Figure 4, it can be seen that the surface slip morphologies of the $[\bar{1}414]$ Ag single crystal are basically comprised of the interactions between the primary and secondary SBs. The interactions will inevitably lead to the mutual obstacles of the moving dislocation. But in fact, only some obstacles will eventually provide the resistance of the dislocation movement. The resistance increase will result in the increase of the saturation shear stress. So, which obstacles can be transformed into the resistance? To answer this question, the different interactions between the primary and secondary SBs should first be described. Figure 6 shows three different cases of the interactions between the primary and secondary SBs in the $[\bar{1}414]$ Ag single crystal cyclically deformed at a plastic strain amplitude of 1.5×10^{-4} , among which interactions (1) and (2) can be classified as strong interactions, and interaction (3) can be regarded as

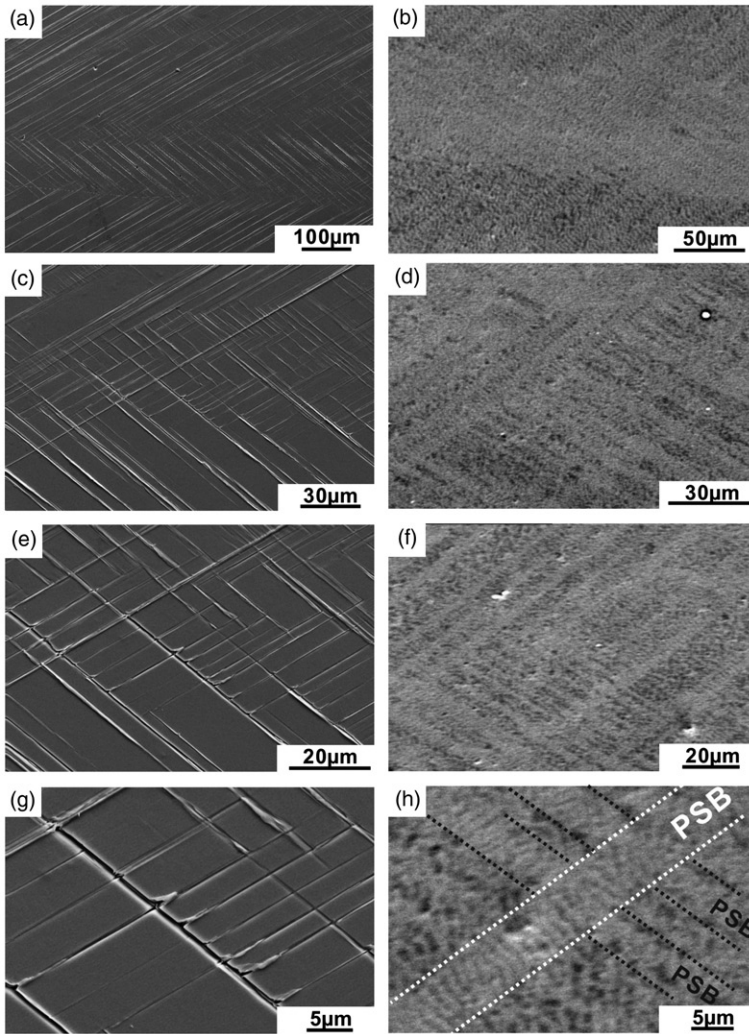


Figure 5. Surface slip morphologies and the corresponding dislocation configurations in the $[1\ 4\ 14]$ Ag single crystal under different magnifications after cyclic saturation at the plastic shear strain amplitudes of 5.0×10^{-4} : (a, c, e, g) the surface slip morphologies; (b, d, f, h) the dislocation configurations.

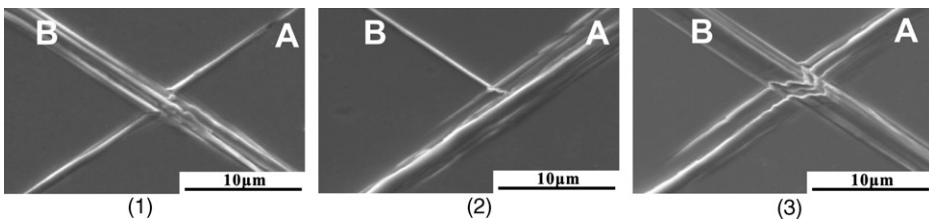


Figure 6. Interaction diagrams between the primary and secondary SB in the $[\bar{1}\ 4\ 14]$ Ag single crystal cyclically deformed at a plastic strain amplitude of 1.5×10^{-4} .

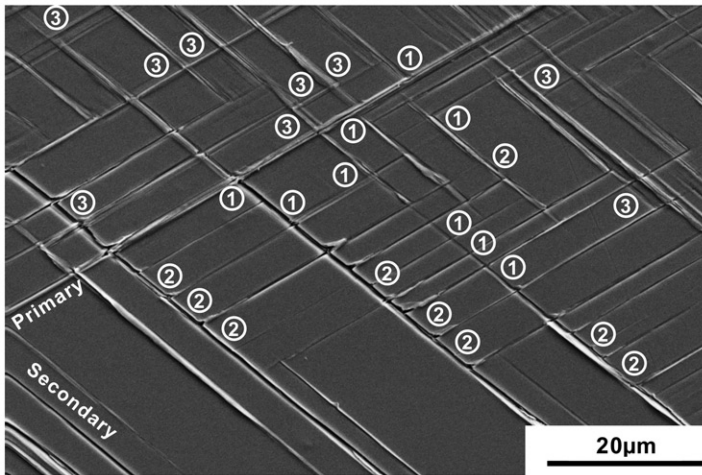


Figure 7. Distribution map of three types of interactions between the primary and secondary SBs according to the slip intensity in the $[\bar{1}414]$ Ag single crystal at a plastic strain amplitude of 5.0×10^{-4} .

a weak interaction. However, the strong interaction will hinder further interaction of dislocations just like dislocation locks in the conjugate double-slip-oriented single crystal.

It has been shown that the saturation stress of the conjugate double-slip-oriented Cu or Ag single crystal is similar to the single-slip-oriented one (see Table 3). Therefore, although the first two interactions increase the local strength, they have no significant contribution to the average saturation shear stress. Only the third case can ensure that the interactions of a large number of single dislocations occur continuously, which is the main reason for the increase of saturation stress.

Figure 7 shows the morphology of the $[\bar{1}414]$ Ag single crystal at the plastic strain amplitude of 5.0×10^{-4} . As pointed out above, the interactions between the primary and secondary SBs are most apparent at this strain amplitude, so all the three morphologies above appeared in different local areas, and are marked with (1), (2) and (3), respectively. This indicates that despite being under the same cyclic deformation condition, the local slip appearances in the same single crystal are quite different, which just verified the effect of the slippage on the interaction mode between the primary and secondary SBs. In Figure 7, it can be seen that the appearance probabilities of three cases are approximately the same. Thus, it can be concluded that the basic reason for increasing the saturation shear stress is the interaction between the primary and secondary SBs, but how can the above judgment be quantified? Maybe the two-phase model should first be mentioned.

4.2. Two-phase model for PSB-ladder structures

As mentioned in Section 3.3, in the $[\bar{1}414]$ Ag single crystal the distribution of PSBs is in rough agreement with the primary and secondary SBs. Here, we will further

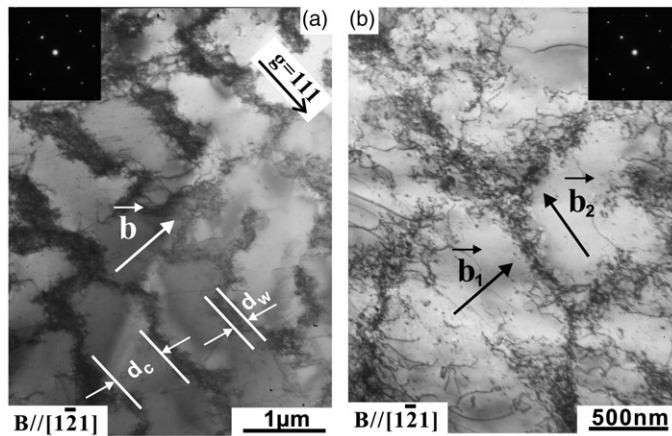


Figure 8. The wall structures observed in the $[\bar{1}414]$ Ag single crystal cyclically deformed at $\gamma_{pl} = 5.0 \times 10^{-4}$, $(1\bar{2}1)$ foil: (a) primary PSB wall; (b) primary and secondary PSB wall.

Table 4. Saturation stress values and physical or geometrical parameters of PSBs in Cu and Ag single crystals with single-slip or critical double-slip orientations.

Metal (orientation)	τ_s^E (MPa)	G (GPa)	SFE γ_{sf} (mJ m ⁻²)	b_1 (Å) b_2 (Å)	d_c (μm)	d_w (μm)	f_w %	τ_s^T (MPa)
Cu (single slip)	27.5	31–75 (40)	40–78 (40)	2.55	1.2	0.15 ± 0.02		29
Cu ([012])	31.4	31–75 (40)	40–78 (40)	2.55	1.5	0.15 ± 0.02	~1	32.9
Ag (single slip)	17.5	19–44 (30)	16–22 (20)	2.50	1 ± 0.2	0.1 ± 0.02	0	~20
Ag (~[027])	26.6	19–44 (25)	16–22 (20)	2.50	1 ± 0.2	0.1 ± 0.02		28.1
References	[4,5,22]	[47]	[48–51]	[51]	[5,6,21,22]			

Note: $f_w = d_w / (d_c + d_w)$; the numbers in parenthesis represent the value actually selected in calculation. For example, the selection of the elastic modulus G bases on the principle that the denser the atomic arrangement is, the higher the elastic modulus is.

discuss the interactions between the dislocation configurations of Ag single crystal with nearly critical double-slip orientation and the influence of the interaction on the saturation resolved shear stress.

Firstly, the geometrical parameters of PSB walls should be obtained, including channel width, d_c , wall thickness, d_w , and the area fraction, f_w , of walls. Figure 8 shows the parameters and dislocation patterns in detail. It can be seen that when the incident beam direction is $B//[1\bar{2}1]$, as shown in Figure 8a, the typical ladder-like PSBs appear in the Ag single crystal similar to those in Cu single crystals [22]. In addition, because the orientation of the Ag single crystal is close to the critical double-slip system, secondary PSBs with ladder-like structure can also be seen, as shown in Figure 8b. The Burgers vectors of the primary and secondary SBs are marked by b_1 and b_2 , respectively. Along the Burgers vectors, the geometrical parameters of primary and secondary SBs can be determined (see Table 4).

Secondly, according to Figures 5 and 8, it can be clearly seen that the PSB can be regarded as a composite consisting of ladder-like walls and channels between them,

so Mughrabi et al. [35,36] presented the theoretical formula of the plateau stress τ_s in terms of the two-phase model:

$$\tau_s = f_w \tau_w + (1 - f_w) \tau_c, \quad (1)$$

where τ_c and τ_w are the flow stresses of the channels and the walls, respectively, and f_w is the area fraction of the walls. In order to apply this formula to calculate the plateau saturation resolved shear stress, we utilized the concept of “unit dislocation configuration” [21]. It is believed that the unit structure of ladder-like walls approximating to an equilateral triangle is composed of two pairs of dipoles with positive–negative edge partial dislocations and an extended dislocation. The concept is similar to the faulted dipoles, which was first mentioned by Hirsch [37] and subsequently analyzed by Seeger [38] and Steeds [39,40]. In the 1970s, Antonopoulos et al. [41,42] expanded the concept of faulted dipoles to study the fatigue behavior of fcc crystals. They thought that all, or nearly all, of the faulted dipoles were vacancy dipoles in the Z configuration, is consistent with our judgment [21]. Therefore, combined with the solving formula of the flow stress τ_c and τ_w from the literature [13,43], the final equation can be simplified as [21]

$$\tau_s/G = \frac{M}{G/\gamma_{sf}} + \frac{N}{d_c}, \quad (2)$$

where

$$M = \frac{2f_w}{3(2 - \nu)b} \quad (3)$$

and

$$N = \frac{8(1 - f_w)b}{3}. \quad (4)$$

Thus, the whole equation consists of the three components, i.e. τ_s/G , G/γ_{sf} and d_c , where τ_s/G denotes the difficulty degree of slip, G/γ_{sf} indicates the ability of the stacking fault aggregation and d_c denotes the geometrical structure of PSBs.

4.3. Dislocation interaction model between PSBs

The above formula gives the criterion for the formation of PSBs in fcc single crystals with single-slip orientation. However, for the fcc single crystals with double-slip orientations, this formula is not good enough and needs to be further improved. It is well known that double-slip systems can be classified into three modes: conjugate, critical and coplanar. Their dislocation reactions are as follows [8]:

- (1) Conjugate dislocation reactions produce stable and non-slip Lomer–Cottrell dislocation locks [44,45], the reaction of which is strong. Thus, although two sets of two-phase PSB structures form in their respective regions [7], under strong hindrance by dislocation locks, PSBs from the conjugate system mostly terminate in PSBs from the primary system (similar to the case in interaction (2) of Figure 6 and the results from Li et al. [32]). If so, the flow stress field from the primary system can not have been affected significantly,

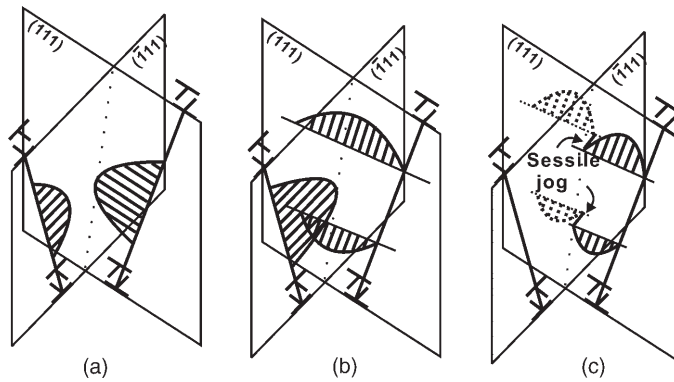


Figure 9. Schematic forming processes of sessile jogs between single screw dislocations: (a) before intersection of dislocations; (b) intersection of dislocations; (c) formation of jogs.

which is the reason why its saturation stress is close to that of the single crystal with single-slip orientation. Hence, dislocations with two slip systems can freely move and proliferate in their respective regions and eventually form independent PSBs, as shown in Figures 5b, 5d, 5f and 5h.

- (2) In contrast, a coplanar dislocation moves and proliferates in the same region, so its reaction is more complex than the other two (see Jin et al. [5,6] and Li et al. [12]).
- (3) Critical dislocation reactions produce sessile jogs. Compared with dislocation locks, the reaction intensity of sessile jogs is weak. Therefore, the dislocations will overcome the resistance to keep the interaction, which is the main difference between the critical and conjugate dislocations [6,7]. In this case, PSBs with the critical system can be fully developed as well as those with the primary system, the typical morphology of which is shown by interaction (3) of Figure 6. Here, both sets of SBs are fully developed and form stable PSB-ladder structures (see in Figure 5h) but still retain the interaction. The interaction derives from the intersection between the screw dislocations with two slip systems that moved between PSB ladders. So the resistance from the sessile jogs formed by the intersection is added to the original flow stress field, which results in an increase in the saturation stress. Hence, dislocations with two slip systems can move and proliferate in their respective regions with interference with each other, and eventually form PSBs that interact with each other.

This paper has just dealt with the third case. Based on the analysis above, it is clear that the intersection between two sets of screw dislocations among PSB ladders can be regarded as the basic reason for a slight increase in the plateau stress compared with typical single-slip-oriented Ag single crystals. However, in order to further analyze the effect of the jog hindrance on the plateau stress, it is necessary to understand the formation of sessile jogs between PSB ladders based on single screw dislocation. Firstly, Figure 9 presents the entire processes in the formation of sessile jogs between screw dislocations. Figure 9a shows the bowing-out dislocation segments along the primary edge dislocation lines. Furthermore these dislocation

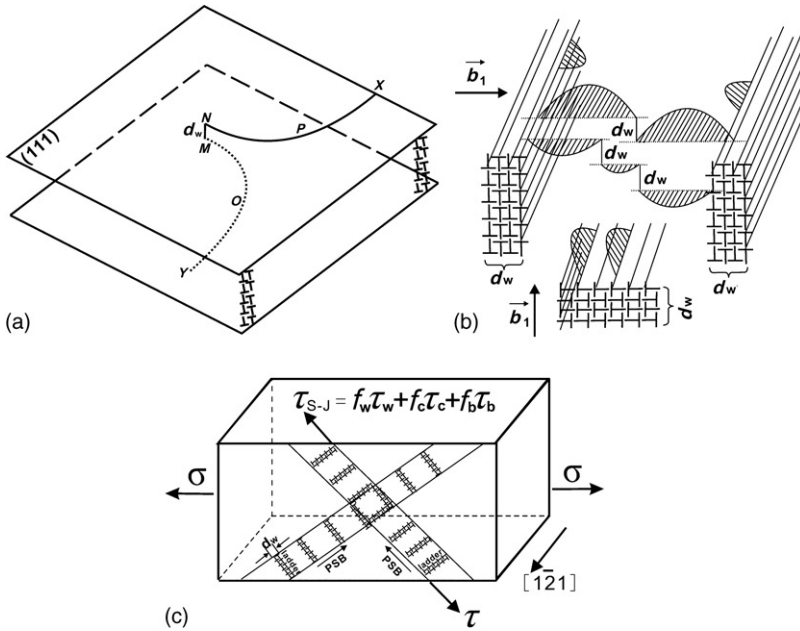


Figure 10. Sketch map of the accumulation effect on the sessile jogs: (a) sessile jogs on the screw dislocation line in the flow stress field; (b) formation of jogs group between PSBs ladders; (c) three items constituting the saturation stress.

segments continue to slip and gradually develop into the screw dislocation, as shown in Figure 9b. In the process of the reciprocating movement of the screw dislocations in the channel, the bowing-out dislocation from the critical slip system will intersect with the screw dislocations from the primary slip system (see Figure 9b). The formation of the sessile jogs is due to these intersections, which causes the obstruction to the subsequent dislocation movement (Figure 9c).

Secondly, Figure 10a shows the sessile jogs on the screw dislocation line in the flow stress field. To some extent, the length of jogs is dominated by the action of the screw dislocation with the other slip system, and the action is directly related to the width of PSB ladders. Therefore, it can be roughly assumed that the length of jogs is equivalent to the width of PSB ladders. Finally, between the actual PSB ladders, jog groups are exhibited, but it is unchanged for a single jog's contribution to the flow stress field. As shown in Figure 10b, the formation of jog groups between PSB ladders will be achieved and the hindrance item of sessile jogs can be expressed as (see Hull and Bacon [46])

$$\tau_b = \frac{0.25 Gb}{2\pi(1 - \nu) y}, \tag{5}$$

where y can be replaced by d_w . For the critical double-slip-oriented crystals, it can be regarded that their saturation stress is composed of three items (see Figure 10c), the two items from the two-phase model plus the hindrance item of sessile jogs.

So based on Equation (1), the saturation resolved shear stress can be further expressed as

$$\tau_{S-J} = \tau_S + \tau_J = f_w \tau_w + f_c \tau_c + f_b \tau_b, \quad (6)$$

where τ_J denotes the contribution of flow stress of sessile jogs to the saturation stress; f_b can be estimated according to the distribution of three types of interactions in Figure 7.

On the assumption that a PSB ladder consists of the interactions completely, the proportion of the third type is approximately 33%. Ultimately, substituting Equations (2) and (5) into Equation (6), the saturation stress can be further simplified as

$$\tau_{S-J}/G = \frac{M}{G/\gamma_{sf}} + \frac{N}{d_c} + \frac{L}{d_w}, \quad (7)$$

where $L = \frac{bf_b}{8\pi(1-n)}$ is a constant. Substituting G , γ and $b \approx 2.5 \text{ \AA}$ [51] into Equation (7), the saturation shear stress can be estimated, as listed in Table 4, wherein τ_s^E and τ_s^T denote the experimental and theoretical values of the saturation shear stresses, respectively. It can be shown that the theoretical values are in good agreement with the experimental ones, especially for the critical double-slip-oriented Cu or Ag crystals, indicating that the above theoretical model is effective for judging the formation of PSBs and estimating the saturation stress value in different fcc crystals.

After plenty of systematic low-cycle fatigue testing under constant plastic strain amplitude, it can be found that most cyclic deformation behaviors of Ag single crystals, as one of the fcc metal crystals, are similar to those of Cu single crystals. Therefore, together with Ni single crystal, the three fcc metals can be classified as one family with similar cyclic deformation behaviors, which are obviously different from those in other fcc single crystals, such as Al, Cu–Al and Cu–Zn, etc. Such similarities and differences are correlated with the stacking fault energy (SFE) of the fcc crystals. In a word, from this point of judging the cyclic deformation behaviors according to the SFE value, fcc single crystals can be divided into three classes: Al crystal with high SFE; Cu, Ni and Ag crystals with moderate SFE; and Cu–Al and Cu–Zn crystals with the lower SFE. In the end, it is worth paying close attention to the questions about: why the level of SFE can significantly affect the cyclic deformation behaviors of various fcc crystals and whether the SFE can be looked upon as only criterion measuring the difference or not, which may be discussed in a forthcoming paper.

5. Conclusions

- (1) The CSS curve of the $[\bar{1}414]$ Ag single crystal shows a clear plateau region over a resolved shear strain amplitude range of $\gamma_{pl} = 1.5 \times 10^{-4} - 4 \times 10^{-3}$ with an average saturation resolved shear stress of $\sim 26.6 \text{ MPa}$. The plateau region is slightly shorter than that of single-slip-oriented Cu single crystal and similar to that of the $[\bar{2}33]$ Ag single crystal.

- (2) Corresponding to the saturation plateau region, ladder-like PSBs appear in the [1414] Ag single crystal and the distribution of PSBs is in rough agreement with the primary and secondary SBs.
- (3) Using the difference of the slippage between the primary and secondary SBs, the interactions can be divided into three types: the secondary SBs run through the primary SBs; the secondary SBs terminate at the edge of the primary SBs; the secondary SBs and the primary SBs tangle up, but go through each other.
- (4) The saturation stresses of the critical double-slip-oriented single crystals, no matter whether for Cu or Ag, are significantly higher than that of single-slip-oriented one. Combining the two-phase model with the hindering effect of sessile jogs on screw dislocation movement, a new three-phase model is proposed to explain the increase in the saturation stress of the critical double-slip-oriented single crystals.

Acknowledgements

The authors would like to acknowledge H.H. Su, W. Gao, L.X. Zhang and H.F. Zou for the assistance in the fatigue experiments, slip morphology and dislocation observations. This work was financially supported by the "Hundred of Talents Project" of Chinese Academy of Sciences and the National Outstanding Young Scientist Foundation under Grant No. 50625103, and the National Basic Research Program of China under Grant No. 2010CB631006.

References

- [1] S.J. Basinski, Z.S. Basinski and A. Howie, *Phil. Mag.* 19 (1969) p.899.
- [2] A.T. Winter, *Phil. Mag.* 30 (1974) p.719.
- [3] J.M. Finney and C. Laird, *Phil. Mag.* 31 (1975) p.339.
- [4] H. Mughrabi, *Mater. Sci. Eng.* 33 (1978) p.207.
- [5] N.Y. Jin, *Phil. Mag.* 48 (1983) p.L33.
- [6] N.Y. Jin and A.T. Winter, *Acta Metall.* 32 (1984) p.989.
- [7] N.Y. Jin, *Acta Metall. Sin.* 24 (1988) p.299.
- [8] N.Y. Jin, *Acta Metall. Sin.* 24 (1988) p.311.
- [9] B. Gong, Z.G. Wang and Y.M. Zhang, *Mater. Sci. Eng. A* 194 (1995) p.171.
- [10] B. Gong, Z.R. Wang, Z.G. Wang and Y.M. Zhang, *Mater. Sci. Eng. A* 210 (1996) p.94.
- [11] X.W. Li, Y. Umakoshi, B. Gong, S.X. Li and Z.G. Wang, *Mater. Sci. Eng. A* 333 (2002) p.51.
- [12] X.W. Li, Z.G. Wang, Y.W. Zhang, S.X. Li and Y. Umakoshi, *Phys Status Solidi (a)* 191 (2002) p.97.
- [13] J. Bretschneider, C. Holste and B. Tippelt, *Acta Mater.* 45 (1997) p.3775.
- [14] C. Buque, *Int. J. Fatigue* 23 (2001) p.671.
- [15] J.C. Grosskreutz and H. Mughrabi, in *In Constitutive Equations in Plasticity*, A.S. Argon, ed., MIT Press, Cambridge, MA, 1975, pp.251–326.
- [16] C. Laird, P. Charsley and H. Mughrabi, *Mater. Sci. Eng.* 81 (1986) p.433.
- [17] Z.S. Basinski and S.J. Basinski, *Prog. Mater. Sci.* 36 (1992) p.89.
- [18] C. Hostle, *Phil. Mag.* 87 (2004) p.299.
- [19] Z.F. Zhang and Z.G. Wang, *Prog. Mater. Sci.* 53 (2008) p.1025.

- [20] P. Li, Z.F. Zhang, S.X. Li and Z.G. Wang, *Acta Mater.* 56 (2008) p.2212.
- [21] P. Li, Z.F. Zhang, S.X. Li and Z.G. Wang, *Scripta Mater.* 59 (2008) p.730.
- [22] H. Mughrabi, F. Ackermann and K. Herz, in *Fatigue Mechanisms*, J.T. Fong, ed., ASTM STP 675, ASTM, Philadelphia, 1979, pp.69–105.
- [23] R. Zauter, F. Petry, M. Bayerlein, C. Sommer, H.J. Christ and H. Mughrabi, *Phil. Mag.* 66 (1992) p.425.
- [24] A. Schwab, J. Bretschneider, C. Buque, C. Blochwitz and C. Holste, *Phil. Mag. Lett.* 74 (1996) p.449.
- [25] D. Melisova, B. Weiss and R. Stickler, *Scripta Mater.* 36 (1997) p.1061.
- [26] J. Ahmed, A.J. Wilkinson and S.G. Roberts, *Phil. Mag. A* 81 (2001) p.1473.
- [27] Z.F. Zhang and Z.G. Wang, *Phil. Mag. Lett.* 78 (1998) p.105.
- [28] Z.F. Zhang, Z.G. Wang and Y.M. Hu, *Scripta Mater.* 40 (1999) p.1353.
- [29] Z.F. Zhang, Z.G. Wang and Z.M. Sun, *Acta Mater.* 49 (2001) p.2875.
- [30] Z.F. Zhang and Z.G. Wang, *Acta Mater.* 51 (2003) p.347.
- [31] X.W. Li, Z.G. Wang, G.Y. Li, S.D. Wu and S.X. Li, *Acta Mater.* 46 (1998) p.4497.
- [32] X.W. Li, Z.G. Wang and S.X. Li, *Mater. Sci. Eng. A* 269 (1999) p.166.
- [33] X.W. Li, Z.G. Wang and S.X. Li, *Mater. Sci. Eng. A* 265 (1999) p.18.
- [34] X.W. Li, Z.G. Wang and S.X. Li, *Mater. Sci. Eng. A* 260 (1999) p.132.
- [35] H. Mughrabi, in *Continuum Models of Discrete Systems*, Proceedings of the Fourth International Conference on Continuum Models of Discrete Systems, O. Brulin, R.K.T. Hsieh, eds., 1981, pp.241–257.
- [36] H. Mughrabi, *Acta Metall.* 31 (1983) p.1367.
- [37] P.B. Hirsch, *The Relation Between Structure and Mechanical Properties of Metals*, HMSO, London, 1963, pp.48–82.
- [38] A. Seeger, *Discuss. Faraday Soc.* 38 (1964) p.82.
- [39] J.W. Steeds, *Phil. Mag.* 16 (1967) p.771.
- [40] J.W. Steeds, *Phil. Mag.* 16 (1967) p.785.
- [41] J.G. Antonopoulos and A.T. Winter, *Phil. Mag.* 33 (1976) p.87.
- [42] J.G. Antonopoulos, L.M. Brown and A.T. Winter, *Phil. Mag.* 34 (1976) p.549.
- [43] U. Essmann and K. Differt, *Mater. Sci. Eng. A* 208 (1996) p.56.
- [44] W.N. Lomer, *Phil. Mag.* 42 (1951) p.1327.
- [45] A.H. Cottrell, *Phil. Mag.* 43 (1952) p.645.
- [46] D. Hull and D.J. Bacon, *Introduction to Dislocations*, 3rd ed., Pergamon Press, Oxford, 1984, pp.157–161.
- [47] Z.S. Hou and G.X. Lu, *Principles of Metallography*, Shanghai Science and Technology Press, Shanghai, 1990, p.174.
- [48] Z.R. Wang, *Phil. Mag.* 84 (2004) p.351.
- [49] M. Rester, C. Motz and R. Pippan, *Scripta Mater.* 58 (2008) p.187.
- [50] L.E. Murr, *Interfacial Phenomena in Metals and Alloys*, Addison-Wesley, Reading, MA, 1975, pp.145–148.
- [51] D.Z. Yang, *Dislocation and Metal Strengthening Mechanism*, Harbin Institute of Technology Press, Harbin, 1991, p.71.